Photodynamic agents with anti-metastatic activities

Vummidi, B R ; Noreen, F ; Alzeer, J ; Moelling, K ; Luedtke, N W

Abstract: A new concept in multifunctional anticancer agents is demonstrated. Tetrakis-(diisopropylguanidino) zinc phthalocyanine (Zn-DIGP) exhibits excellent properties as a photodynamic therapy (PDT) agent, as well as potential anti-metastatic activities in vivo. Zn-DIGP exhibits good cellular uptake and low toxicity in the dark (EC50 > 80 M) and is well tolerated upon its intravenous injection into mice at 8 mg/kg. Upon photoexcitation with red laser light (660 nm), Zn-DIGP exhibits a high quantum yield for singlet oxygen formation (0.51) that results in potent phototoxicity to cell cultures (EC50 0.16 M). Zn-DIGP is also capable of inhibiting the formation of tumor colonies in the lungs of C57BL/6 mice injected with B16F10 cells. Zn-DIGP therefore inhibits cancer growth by both light-dependent and light-independent pathways. The anti-metastatic activities of Zn-DIGP possibly result from its ability to interfere with the signaling between chemokine CXCL10 and the G protein-coupled receptor CXCR3. Zn-DIGP is a competitive inhibitor of CXCR3 activation (IC50 = 3.8 M) and selectively inhibits downstream events such as CXCL10-activated cell migration. Consistent with the presence of feedback regulation between CXCR3 binding and CXCL10 expression, Zn-DIGP causes overexpression of CXCL10. Interestingly, Zn-DIGP binds to CXCR3 without activating the receptor yet is able to cause endocytosis and degradation of this GPCR. To the best of our knowledge, Zn-DIGP is the first PDT agent that can facilitate the photodynamic treatment of primary tumors while simultaneously inhibiting the formation of metastatic tumor colonies by a light-independent mode of action.

DOI: https://doi.org/10.1021/cb400008t

Photodynamic Agents with Anti-Metastatic Activities

*Balayeshwanth R. Vummidi,[†] Faiza Noreen,[‡] Jawad Alzeer,[†] Karin Moelling,[‡] and Nathan W. Luedtke[†]**

[†] Department of Chemistry, University of Zurich, Winterthurerstrasse 190, CH-8057, Zurich Switzerland, [‡] Institute of Medical Virology, University of Zurich, Gloriastrasse 30, CH-8006 Zurich, Switzerland

RECEIVED DATE

TITLE RUNNING HEAD: Photodynamic anti-metastatic agents

Keywords: Phthalocyanine, cancer, chemokine, CXCL10-CXCR3, GPCR antagonist.

* To whom correspondence should be addressed. Phone: + 41 44 635 4244 Fax: + 41 44 635 6891 E-mail: luedtke@oci.uzh.ch † Department of Chemistry, University of Zurich ‡ Institute of Medical Virology, University of Zurich

ABSTRACT

A new concept in multifunctional anti-cancer agents is demonstrated. Tetrakis-(diisopropyl-guanidino) zinc phthalocyanine "Zn-DIGP" exhibits excellent properties as a photodynamic therapy (PDT) agent, as well as potential anti-metastatic activities *in vivo*. Zn-DIGP exhibits good cellular uptake and low toxicity in the dark (EC_{50} > 80 μM), and is well tolerated upon its intravenous injection into mice at 8 mg / kg. Upon photoexcitation with red laser light (660 nm), Zn-DIGP exhibits a high quantum yield for singlet oxygen formation ($\Phi \approx 0.51$) that results in potent phototoxicity to cell cultures ($EC_{50} \approx 0.16$ μM). Zn-DIGP is also capable of inhibiting the formation of tumor colonies in the lungs of C57BL/6 mice injected with B16F10 cells. Zn-DIGP therefore inhibits cancer growth by both light-dependent and light-independent pathways. The anti-metastatic activities of Zn-DIGP possibly result from its ability to interfere with the signaling between chemokine CXCL10 and the G protein-coupled receptor CXCR3. Zn-DIGP is a competitive inhibitor of CXCR3 activation (IC_{50} = 3.8 μM), and it selectively inhibits downstream events such as CXCL10-activated cell migration. Consistent with the presence of feedback regulation between CXCR3 binding and CXCL10 expression, Zn-DIGP causes overexpression of CXCL10. Interestingly, Zn-DIGP binds to CXCR3 without activating the receptor, yet is able to cause endocytosis and degradation of this GPCR. To the best of our knowledge, Zn-DIGP is the first PDT agent that can facilitate the photodynamic treatment of primary tumors while simultaneously inhibiting the formation of metastatic tumor colonies by a light-independent mode of action.

Skin cancers account for about half of all cancers in the United States, where complications associated with the spread of melanoma to vital organs are a leading cause of death for women aged 19 to 50 years.*(1, 2)* While surgery remains the main treatment option for advanced malignancies,*(3)* early-stage melanoma and non-melanoma skin cancers can be treated with photodynamic therapy (PDT).*(4-6)* Photodynamic therapy involves utilization of photosensitizers that exhibit phototoxicity by two common mechanisms, Type 1 involves long-lived triplet states of the photosensitizer that react directly with cellular components; Type 2 involves formation of singlet oxygen which triggers cell death.*(7)* Many photosensitizing agents have been evaluated in the clinic,*(8, 9)* but only four PDT agents, all of which being porphyrin derivatives, are currently approved by the FDA: Verteporfin (Visudyne®), Porfimer Sodium (Photofrin®), 5-aminolevulinic acid (Luvulan®), and 5-aminolevulinic acid methyl ester (Visudyne®). None of these PDT agents, however, are ideal candidates for treating melanoma. In clinical trials, poor results were obtained when porphyrin-based PDT agents were used to treat melanoma and related maladies.*(10)* One key limitation to these compounds is their relatively short maximal wavelengths of excitation ($\lambda_{max} \approx 630$ nm), where melanin-rich tissues absorb too much light energy to be useful.*(4)* In terms of tissue permeability, photosensitizers with longer wavelengths of excitation should provide better treatment options.*(11)* For example, the chlorin-based derivative e6 ($\lambda_{max} \approx 660$ nm) was successfully used to treat melanoma-derived skin metastases in human patients,*(5)* and a related compound "mono-L-aspartyl chlorin e6" exhibited good efficacy in a Phase II clinical trial.*(12)* Phthalocyanines ($\lambda_{max} \approx 690$ nm) exhibit absorbance into the near-infrared,*(13)* and can therefore utilize longer wavelengths of light than porphyrins and chlorins for better tissue permeability.

The photophysical properties of phthalocyanines are known to be strongly influenced by the centrally-coordinated metal ion. For example, copper-containing phthalocyanines are essentially photo-inert and used as tattoo inks; while aluminum, silicon, and zinc-containing phthalocyanines are highly phototoxic.*(14)* Zinc and silicon-containing phthalocyanines have exhibited promising PDT activities in pre-clinical and phase-I clinical trials for chroidal neovascularization and cutaneous neoplasms.*(15, 16)* However, the notorious insolubility and

aggregation properties of phthalocyanines can negatively affect their cellular uptake and ability to act as photosensitizers.*(17)* Given these limitations, efforts have been directed towards the synthesis of water soluble and cell-permeable phthalocyanine derivatives.*(18)* For example, we recently synthesized a new family of cationic phthalocyanines termed "guanidino phthalocyanines" (GPcs) containing four guanidinium groups.*(19)* One such derivative, tetrakis-(diisopropyl-guanidine) zinc phthalocyanine "Zn-DIGP" exhibits good cellular uptake and the ability to modulate gene expression.*(20, 21)* Presumably as a result of its high affinity binding interaction with a G-quadruplex from the c-myc promoter (K_d < 2 nM), Zn-DIGP can knock-down c-myc transcription at subtoxic doses in time-dependent manner.*(20)* The c-myc oncogene encodes for a transcription factor that, together with ATF-2, plays an important role in proliferation, differentiation and apoptosis of melanoma.*(22)* Abnormal c-Myc expression can lead to tumorigenesis,*(23)* and the inhibition of c-Myc in mouse models causes melanoma regression.*(24)* Given these results, we decided to evaluate the anti-metastatic activities of GPcs *in vivo*.

Here we report that Zn-DIGP inhibits the formation of metastatic tumor colonies in the lung tissues of mice injected with B16F10 cells. Contrary to our expectations, this inhibition appears to proceed via a G-quadruplex independent mode of action. According to cell-based studies, the anti-metastatic activities of Zn-DIGP are probably a result of its ability to disrupt signaling between chemokine CXCL10 and its receptor CXCR3.*(25-27)* Zn-DIGP binds to CXCR3 and inhibits CXCL10-induced receptor activation with an IC_{50} = 3.8 μM. Unlike previously reported CXCR3 antagonists, Zn-DIGP also exhibits potent phototoxicity as well as the ability to cause CXCR3 endocytosis and degradation. Taken together, these results suggest that Zn-DIGP and other GPcs may serve as multi-functional PDT agents, where light energy can be harnessed for the treatment of primary surface tumors while simultaneously inhibiting the formation of new tumor colonies by interfering with chemokine signaling.

RESULTS AND DISCUSSION

GPcs: Photophysical Properties and Phototoxicity

During our initial synthesis of guanidino phthalocyanines (GPcs), a new de-metallation reaction that furnished tetrakis-(diisopropyl-guanidine) phthalocyanine "DIGP" (**1**) as a single regioisomer was discovered.*(19, 20)* Metal ions such as Zn(II), Cu(II), Co(II), and Pd(II) can be inserted into **1** to give Zn-DIGP (**2**), Cu-DIGP (**3**), Co-DIGP (**4**), and Pd-DIGP (**5**), respectively (Figure 1). Compounds **1** – **5** exhibit excellent solubility and obey Beer's law in DMSO over a concentration range of 0.3 – 5 μM (see Supporting Information, Supplementary Figures S1-S2 for absorbance, excitation and emission spectra). We therefore measured the quantum yields for photon emission and singlet oxygen generation of **1** – **5** in DMSO (Table 1). The known zinc phthalocyanines "Zn-Pc" (**6**) and zinc phthalocyanine tetrasulfonate "Zn-PcS4" (**7**) were included as reference compounds. The quantum yield of Zn-DIGP for luminescence ($\Phi = 0.28$) was more than 100-fold higher than the other metal-containing DIGPs (Table 1). The bright emissions from Zn-DIGP facilitate its direct visualization in cells using fluorescence microscopy. Upon its addition to living B16F10 cells, strong staining of perinuclear organelles and trafficking vesicles by Zn-DIGP can be observed (Figure 2 A-C). No measurable change in cellular respiration was observed in these samples, consistent with the minimal toxicity of Zn-DIGP under conditions of ambient light (Figure 3A, (-) laser). Similar to guanidinium-rich peptides that are known to enter cells *via* endocytosis,*(28)* Zn-DIGP co-localizes with "Lysotracker" in living cells (Supplementary Figure S3). Upon irradiation with 20 joules of far-red light (660 nm), Zn-DIGP-treated cells exhibit large morphological changes and the loss of cellular respiration, consistent with phototoxicity (Figure 3A, (+) laser). Interestingly, a redistribution of Zn-DIGP from the endosomes and lysosomes of living cells to the nuclei of dying cells was observed following irradiation (Figure 2 D-F). This behavior is consistent with endosomal escape and accumulation of Zn-DIGP at high-affinity DNA binding sites upon cell death. Together these results suggest that Zn-DIGP is not freely diffusible across plasma membranes and it therefore has limited access to nuclear DNA in living cells.

The cytotoxic and phototoxic activities of Zn-DIGP were quantified using a standard Alamar Blue assay that reports the combined effects of proliferation and metabolism on total cellular

respiration. B16F10 cells were treated with variable concentrations of **1** – **7** for 24 hours and irradiated with a 660 nm laser (250 mW) for 90 seconds. Three hours later, resazurin was added and its metabolic conversion into resorufin was compared with untreated cells to determine EC_{50} values (see Figure 3A for representative data). A comparison of EC_{50} values for irradiated (+*hv*) versus non-irradiated samples (-*hv*) reveals the relative phototoxicity of each compound (Table 1). The metal-free compound "DIGP" (**1**) shows no significant change in cytotoxicity upon irradiation ($EC_{50} \approx 30$ μM), whereas the metal-containing derivatives **2** – **7** all exhibit minimal dark toxicity ($EC_{50} > 80$ μM) and highly variable toxicity upon irradiation ($EC_{50} = 0.2 – 80$ μM, Table 1). Of all derivatives tested, Zn-DIGP exhibits the most potent phototoxicity, with more than a 400-fold decrease in EC_{50} value ($EC_{50} = 0.16$ μM) upon irradiation. According to these results, Zn-DIGP is approximately 20-times more phototoxic than the well-studied anionic phthalocyanine "Zn-PcS4" (**7**).*(29, 30)*

To determine the probable mechanism of Zn-DIGP's phototoxicity, the quantum yield of singlet oxygen was measured for compounds **1** – **7** by monitoring the time-dependent photobleaching of 1,3-diphenyl isobenzofuran (DPBF).*(31)* Consistent with the low quantum yields of singlet oxygen formation reported for other metal-free phthalocyanines,*(32-34)* DIGP exhibits very little photobleaching of DPBF (Figure 3B), and no changes in cytotoxicity were observed upon irradiating DIGP-treated cells (Table 1). Consistent with "Type 2" photosensitization in cells, the quantum yields for singlet oxygen formation of each M-DIGP derivative correlates with its relative phototoxicity, where Zn > Pd >> Cu / Co (Figure 3B, Table 1). This trend can be explained by the magnetic properties of each metal-containing phthalocyanine.*(34)* Derivatives containing paramagnetic ions (copper, cobalt) generate little or no detectable singlet oxygen, whereas derivatives containing diamagnetic metal ions (palladium and zinc) exhibit high quantum yields for singlet oxygen ($\Phi = 0.41$ and 0.51, respectively). Since all three of the Zn-containing phthalocyanines (**2, 6,** and **7**) exhibited similar quantum yields for singlet oxygen formation ($\Phi \approx 0.5 – 0.6$), the large differences in phototoxicity between Zn-DIGP ($EC_{50} = 0.16$ μM) and Zn-PcS4 ($EC_{50} = 2.7$ μM) are likely due to differences in their cellular uptake.*(17)*

Zn-DIGP: Anti-Metastatic Activities *In Vivo*

Previous studies have demonstrated that Zn-DIGP can knock-down transcription of the c-myc oncogene 3-fold or more in cell cultures.*(20)* Given the important functions of c-myc in mediating melanoma metastasis,*(22-24, 35, 36)* we decided to evaluate the anti-metastatic activities of Zn-DIGP using an assay that mimics the hematogenous spread of malignant melanoma *in vivo*. *(39)* C57BL/6 mice were intravenously injected into the tail vein with B16F10 cells, and after 20 days the animals were sacrificed and the number of lung metastases determined by visual inspection. Control animals receiving untreated cells or cells treated with carrier only (sodium trifluoroacetate in DMSO) contained 38 ± 8 (average ± standard deviation) lung metastases on day 20. Cell cultures that were pre-treated with 5 μM of Zn-DIGP prior to their injection into the mice were incapable of establishing lung tumors (Figure 4, Supplementary Figure S4). Importantly, no changes in cellular respiration or proliferation of the cells were observed at this concentration of Zn-DIGP (Figure 3A, (-) light). In a second, more stringent experimental design (type B), untreated B16F10 cells were injected into the animals on day one, and a solution of Zn-DIGP was injected into the animals at 8 mg / kg on day two. All Zn-DIGP-treated animals reacted well to the injection, showed no signs of stress, and survived the duration of the experiment to day 20. In this experiment, the intravenous application of Zn-DIGP caused an approximate 50% reduction in the number and size of lung metastases on day 20 (Figure 4, Supplementary Figure S4).

Microarray, qRT-PCR, and ELISA for Mechanistic Lead Identification

To provide a relatively unbiased approach for identifying the probable mechanism(s) of Zn-DIGP's anti-metastatic activities, its impact on global gene expression was evaluated using microarray analyses. Compared to B16F10 cells treated with cisplatin,*(39)* Zn-DIGP-treated cells exhibited relatively few differentially expressed genes (Supplementary Figure S5). The addition of Zn-DIGP caused only 40 genes to be differentially expressed with a 2-fold or larger change in mRNA quantities after a 24 hour treatment. Putative G-quadruplex sequences were mostly absent in the promoter regions of these 40 genes. qRT-PCR experiments confirmed that Zn-DIGP caused little or no change in the transcription of c-myc and other genes containing putative G-quadruplex structures in their promoters such as MTA1, VEGF*(40)* and RB1*(41)* in B16F10 cells (Supplementary Figure S6). The inability of Zn-DIGP to impact global gene expression in a

G-quadruplex-dependent manner is possibly related to its mechanism of cellular uptake that results in limited access to nuclear DNA in living cells (Figure 2 A-C, and Supplementary Figure S3).

Repetition of the microarray analysis in an experiment where the fluorescent dyes on each primer were inverted, revealed only a single differentially expressed gene common to both experimental designs. qRT-PCR experiments confirmed that the addition of Zn-DIGP causes overexpression of CXCL10 in B16F10 cells in both a dose- and time- dependent manner (Figure 5). According to ELISA experiments, the changes in extracellular CXCL10 protein levels upon addition of Zn-DIGP were also dose- and time-dependent (Figure 6). Zn-DIGP caused as much as a 20-fold increase in CXCL10 protein expression upon its addition to B16F10 cells at sub-toxic doses (5 μM in the dark). To the best of our knowledge, Zn-DIGP is the first small molecule reported to induce CXCL10 overexpression.

Zn-DIGP Interference of CXCR3-CXCL10 Signaling

B16F10 cells are known to express both CXCL10 and its receptor CXCR3.*(42)* The high-affinity interaction between CXCL10 and CXCR3 ($K_d \approx 0.2$ nM) is mediated by arginine, lysine and isoleucine residues of CXCL10 that bind to an acidic patch on CXCR3.*(43, 44)* The similar physicochemical properties of CXCL10 and Zn-DIGP, both being hydrophobic cations, indicated that Zn-DIGP might mimic CXCL10 to competitively bind CXCR3. To test this hypothesis, competitive displacement experiments were conducted using immobilized CXCR3 receptors and ^{125}I-labeled CXCL10. As a control, unlabelled CXCL10 was titrated and the apparent K_i (0.57 ± 0.02 nM) was found to be similar to previous reports.*(45)* Using this assay, Zn-DIGP was found to displace ^{125}I-labelled CXCL10 with an apparent K_i of 29 ± 1 μM (Figure 7A).

To evaluate the functional impact of CXCR3 binding by Zn-DIGP, agonist assays were performed by monitoring changes in intracellular calcium levels in Chem 1 cells that overexpress CXCR3. As a control, unlabelled CXCL10 was titrated and the apparent EC_{50} value measured for receptor activation (13 ± 1 nM) was similar to previous reports.*(45)* As shown in Figure 7B,

the addition of Zn-DIGP did not cause any detectable increase in intracellular calcium levels, indicating the absence of CXCR3 activation.

To test the ability of Zn-DIGP to inhibit activation of CXCR3 by CXCL10, Zn-DIGP was incubated with Chem 1 cells for 15 min followed by the addition of 13 nM CXCL10. Reduced calcium levels were observed in Zn-DIGP-treated samples (Figure 7C). The IC_{50} of Zn-DIGP for CXCL10-CXCR3 inhibition was 3.8 ± 0.6 μM. Surprisingly, the IC_{50} for CXCR3 inhibition was almost 8-fold lower than the K_i value for CXCL10 displacement (29 ± 1 μM). This apparent conundrum can be explained by cell surface dynamics and receptor turnover. Since CXCL10 binding is known to initiate internalization of CXCR3,*(46, 47)* we speculated that Zn-DIGP binding might also cause receptor internalization, albeit without receptor activation. To test this possibility, B16F10 cells were treated with Zn-DIGP or CXCL10, and CXCR3 was visualized by immunofluorescence. In both the cases, a dramatic loss of CXCR3 staining was observed after 1 – 2 hours of incubation (Figure 8). The localization of CXCR3 was also distinctly different in treated and untreated cells. In control samples, CXCR3 was distributed over the cell surface, whereas CXCL10- and Zn-DIGP-treated cells exhibited perinuclear CXCR3 accumulation consistent with receptor endocytosis (Figure 8). The differences between Zn-DIGP's IC_{50} value for CXCR3 inhibition (3.8 μM) and CXCR3 affinity (K_i = 29 μM) can therefore be attributed to the ability of Zn-DIGP to bind CXCR3 without activation of the receptor, yet causing endocytosis and degradation of CXCR3. To the best of our knowledge, Zn-DIGP is the first small-molecule GPCR antagonist reported to cause receptor internalization and degradation.

To assess the ability of Zn-DIGP to selectively inhibit CXCR3 downstream signaling, we investigated CXCL10-activated cellular motility using scratch assays (Figure 9).*(25, 48, 49)* As a selectivity control, the chemotactic cytokine CCL21 that binds to receptor CCR7 was included.*(50)* Both CXCL10 and CCL21 stimulate cell migration in the absence of Zn-DIGP ("untreated" samples, Figure 9B). In the presence of 5 μM, the changes in migration indices reveal inhibition of CXCL10-mediated cellular migration, but not of CCL21-activated migration (Figure 9). Similar results were also obtained using matrigel-based invasion assays (Supplementary Figure S7). Interestingly, the same migration index was observed for cells

treated with 5 μM of Zn-DIGP from 2 – 100 nM of added CXCL10 (Figure 9). Together these results are consistent with the ability of Zn-DIGP to selectively inhibit CXCL10-mediated signaling via CXCR3 binding and endocytosis.

CONCLUSIONS

Metastatic melanoma is currently associated with such poor patient outcomes that clinical trial participation has been recommended as standard care.*(51)* One novel approach to the treatment of melanoma malignancy is the utilization of PDT agents for destroying the primary tumor while simultaneously inhibiting the formation of metastases throughout the body. As a proof of principle, we have demonstrated that Zn-DIGP exhibits excellent properties as a PDT agent, as well as the ability to inhibit formation of tumor colonies in the lungs of C57BL/6 mice injected with B16F10 cells. To the best of our knowledge, Zn-DIGP provides the first example of a preclinical candidate possessing both of these properties. While the PDT activities of Zn-DIGP still need to be assessed *in vivo*, previous studies have demonstrated that an octadecyl zinc phthalocyanine "ZnODPc" exhibits tumor-selective accumulation and high phototherapeutic efficacy in Balb/c mice bearing MS-2 fibrosarcoma upon intravenous injection at 2.5 mg/kg.*(52)*

Experiments to characterize the anti-metastatic activities of Zn-DIGP and its potential mode of action were conducted using a concentration of 5 μM, where no changes in cellular respiration or proliferation were observed under conditions of ambient light. Given the extreme side effects of cytotoxic chemotherapies currently used for treating metastatic melanoma,*(51)* the ability of Zn-DIGP to interfere with metastasis formation without indiscriminant cell killing presents a highly attractive possibility. The CXCR3 antagonist “AMG487” was also reported to have little or no impact on cellular proliferation in serum-containing media.*(25, 27)*. Consistent with its low toxicity, AMG487 did not impact local tumor growth or survival *in vivo*, but it was able to inhibit metastasis.*(25)* In the case of Zn-DIGP, the site-specific destruction of the primary tumor can be achieved using laser light activation, while simultaneously inhibiting the formation of new metastases in vital organs by interfering with chemokine signaling.

Zn-DIGP is well-tolerated upon intravenous injection into C57BL/6 mice at 8 mg / kg, where it exhibits a light-independent mode of action by inhibiting the formation of pulmonary metastases. While other modes of action can not be excluded, microarray analyses, qRT-PCR, and ELISA experiments all indicate that Zn-DIGP causes overexpression of CXCL10. The beneficial role of CXCL10 in melanoma regression is well characterized, and it has been attributed to two related functions: 1) enhancement of immune response by natural killer cells,*(53, 54)* and 2) induction of anti-angiogenic signals.*(55)* Previous studies using an adenovirus expression vector demonstrated that B16F1 melanoma tumors overexpressing CXCL10 by 50% exhibited diminished proliferation and invasiveness *in vivo*.*(55)* Upon adding 5 μM of Zn-DIGP to B16F10 cells, we observed a 1,000% increase in CXCL10 production *in vitro*, and an almost total loss of metastatic colony formation *in vivo*.

Interestingly, Zn-DIGP causes CXCL10 overexpression and it inhibits CXCR3 activation when applied to cells. Previous studies have demonstrated that RNAi knock down of CXCR3 causes a reduction in the metastatic activities of B16F10 cells in C57BL/6 mice.*(48)* Likewise, the CXCR3-selective antagonist "AMG487" inhibits metastasis in a breast cancer model.*(25)* According to CXCL10 displacement assays *in vitro*, Zn-DIGP binds to CXCR3 with a modest K_i of only 29 μM, but it exhibits an 8-fold more potent IC_{50} value for CXCR3-CXCL10 inhibition on living cells (IC_{50} = 3.8 μM). The unexpected differences between these values, where $K_i > IC_{50}$, can be explained by the ability of Zn-DIGP to bind CXCR3 without activation of the receptor, yet causing endocytosis and degradation of this GPCR. While there is small handful of peptide antagonists known to cause internalization of GPCRs,*(56, 57)* Zn-DIGP represents, to the best of our knowledge, the first small-molecule GPCR antagonist reported to cause receptor internalization and degradation. Given the exceptionally broad importance of GPCRs as drug targets, this unusual mode of receptor inhibition might provide an attractive direction for the future development of GPCR antagonists.

To the best of our knowledge, Zn-DIGP is the first compound reported to cause both CXCL10 overexpression and CXCR3 inactivation in cell cultures. While the exact relationships between these activities is unknown, previous studies have suggested the presence of complex autocrine signaling and feedback regulation between CXCL10 and CXCR3.*(42)* It is therefore possible

that the Zn-DIGP-mediated inactivation and internalization of CXCR3 is responsible for the overexpression of CXCL10. Previous studies have further demonstrated that the overexpression of CXCL10 or the inhibition of CXCR3 are independently sufficient for causing anti-metastatic effects *in vivo*.(25, 55) The potential therapeutic advantage or disadvantage of a single compound exhibiting both activities will be the subject of future studies.

METHODS

Cell Lines and Media. Murine metastatic B16F10 melanoma cell line were cultured in Dulbecco's modified Eagle's medium (DMEM; Invitrogen) supplemented with 2% heat-inactivated fetal calf serum (FCS) and 100 U/ml of penicillin (Sigma), 100 μg/ml of Streptomycin (Sigma). Cells were grown in 5% CO_2 at 37 °C.

Cytotoxicity and Phototoxicity Studies. B16F10 (~10'000 cells) were seeded in 96 well plates and grown for 24 h prior to their incubation with variable concentrations of compounds **1** – **7** for 24 h. Individual wells were then photoexcited with a 250 mW diode laser (containing a beam spreader to diameter = 1 cm) at 660 nm for 90 seconds. After 3 h of incubation in the dark under standard conditions (Cell Lines and Media section), the cellular media were replaced with fresh media containing 86 μM resazurin (Sigma) and incubated at 37 ºC. Fluorescence intensities were measured after 2 – 4 h using M5 spectrophotometer with excitation at 560 nm, emission at 590 nm, and a 570 nm cutoff filter. All samples were compared to untreated cells to calculate the % decrease in respiration, from which EC_{50} values were calculated.

Microscopy. B16F10 cells (~15'000) were seeded in Labtek 8 chambered plate (Nunc) in media containing 10% FCS. After overnight growth, media was replaced with fresh media containing 3 μM Zn-DIGP and incubated for 24 h. Individual wells were then photoexcited with a 250 mW diode laser (containing a beam spreader to diameter = 1 cm) at 660 nm for 90 seconds. Images of the unfixed cells were collected using Leica LX wide field microscope before irradiation, as well as 3 h following irradiation with a 250 mW diode laser (containing a beam spreader to diameter = 1 cm) at 660 nm for 90 sec.

Animal Studies. C57BL/6 mice were bred in the animal facility of the Institute of Medical Virology, University of Zurich, and used at 6-8 weeks of age. All experiments were conducted

according to the Guide for the Care and Use of Laboratory Animals. Zn-DIGP (trifluoroacetate salt) was diluted into DMSO at a concentration of 10 mM (15.5 mg / mL). Alternatively, as a control vehicle, 40 mM solutions of sodium trifluoroacetate were prepared in DMSO. Zn-DIGP and control solutions were diluted 10-fold into DMEM + 10% FCS to make 1 mM and 4 mM solutions and sterile filtered immediately prior to their application onto cells or injection into mice. In the first series of experiments (type A), B16F10 cell cultures were incubated in standard media containing 5 μM of Zn-DIGP or 20 μM sodium trifluoroacetate and 10% FCS for 16 h. The cells were then trypsinized and washed twice with PBS and diluted to 2 x 10^5 cells in a total volume of 200 μl. The formation of pulmonary metastases was established by intravenous injection of Zn-DIGP-treated or control cells into the tail vein of C57BL/6 mice. Twenty days later, the animals were sacrificed and numbers of lung metastases were examined by visual inspection of lungs.*(37, 38)* In a second series of experiments (type B), 2 x 10^5 cells of B16F10 cells, in 200 μl of PBS were injected into the tail vein of C57BL/6 mice. On the second day, the mice were injected with 100 μL of 1 or 4 mM solutions of Zn-DIGP or sodium trifluoroacetate carrier (prepared in DMEM + 10% FCS as described above). Twenty days later the animals were sacrificed and numbers of metastases were examined by visual inspection of lungs. The results for untreated animals were the same as those receiving the carrier only. The results are shown as numbers of metastases in individual mice. Bars represent relative numbers of metastases +/- standard errors from two independent experiments.

[^{125}I] CXCL10 Displacement Assays. Zn-DIGP was dissolved in DMSO at a concentration of 100 mM and serial dilutions were conducted in DMSO. 60-fold dilutions were then made into an equilibrium binding buffer (water supplemented with 50 mM HEPES, 5 mM $MgCl_2$, 1 mM $CaCl_2$, 0.2% BSA at pH 7.4) to concentrations that were four-fold higher than the final assay concentration. CXCL10 and Zn-DIGP were mixed 1:1 (v/v) with [^{125}I]-CXCL10 to a final concentration of 0.1 nM and added to CXCR3 membranes (Millipore) prepared in assay buffer at 1 unit/well. The assay plate was incubated at rt for 120 min. Prior to CXCL10 capture, the FC filter plate (Millipore) was pre-coated with 0.3% Polyethyleneimine (PEI) for one hour. Following capture, the FC filter plate was washed three times (50 mM HEPES, pH 7.4, 500 mM NaCl, and 0.1% BSA). The filtration plate was allowed to dry and 50 μL per well of scintillation fluid was added and counted on a Perkin Elmer (Wallac) 1450 Microbeta TriLux liquid scintillation counter. K_i values were calculated based on the Cheng-Prusoff equation; $K_i = IC_{50}/[1$

+ ([L]/K_d), where IC_{50} is the half maximal inhibition concentration, [L] is the CXCL10 ligand concentration (0.1 nM), K_d is the measured equilibrium dissociation constant (0.2 nM) of the CXCL10 - CXCR3 binding interaction.

Ca^{2+} Flux Assays. Chem1 cells (~ 50,000) that overexpress CXCR3 were seeded in 96 well plates and incubated at rt for 30 min before transferring to 37 ºC incubator for overnight incubation. Assay buffer (Hanks Balanced Salt Solution containing 20 mM HEPES and 2.5 mM Probenecid; pH = 7.4) and loading buffer (assay buffer + 5 mM Fluo-8 dye) were prepared freshly. The cells were then washed once with assay buffer and incubated with loading buffer for 1.5 h. Meanwhile, Zn-DIGP was dissolved in DMSO at a concentration of 100 mM and serial dilutions were conducted in DMSO. 1000-fold dilutions were made into assay buffer to concentrations three-fold higher than the final assay concentrations. Vehicle only and positive controls were prepared in the same way. The CXCR3 agonist assays were conducted using a $FLIPR^{TETRA}$ instrument where Zn-DIGP, vehicle controls, and reference agonist (CXCL10) were added to assay plates containing the washed Chem1 cells in loading buffer, and Fluo-8 fluorescence was read as a function of time. Upon completion of the agonist assay, the assay plate was removed from the $FLIPR^{TETRA}$ instrument and incubated at 25 °C for 7 min. After the incubation period, the assay plate was placed back into the $FLIPR^{TETRA}$ instrument and the antagonist assay was initiated. The antagonist assay was conducted using the same methodology as the agonist assays. Using the EC_{50} concentration of CXCL10 determined by the agonist assay (13 nM), all pre-incubated Zn-DIGP wells were challenged with CXCL10 after establishment of a fluorescence baseline. Maximum fluorescence values were used to calculate percentage activation, percentage inhibition (relative to EC_{50} and vehicle control values), and additional statistical values (Z`, percentage variation between replicate data values) to assess the quality of each plate. All dose response curves were fit using GraphPad Prism.

Receptor Internalization Assays. B16F10 cells (~70`000) were seeded in 24 well plates containing cover slips in 10% FCS containing media. After 4 h, 10% FCS containing media was replaced with 0% FCS containing media. After overnight incubation, the used media was replaced with fresh 0% FCS containing media and left for 30 min. 0% FCS media containing 20 nM of CXCL10 or 5 μM Zn-DIGP were then added and incubated for 0, 1, or 2 h. Cells were then washed twice with 1 ml of PBS, fixed with 3% PFA for 15 min and washed twice with PBS. Cover slips were stained with CXCR3 primary antibody (Abcam, 1:400 dilution in PBS

containing 0.1% BSA) and incubated at rt for 1 h and washed twice with PBS. Fluroscein-labeled secondary antibody staining was performed with 1:500 dilution of the antibody (Abcam) in PBS containing 0.1% BSA and incubated for 1 h at rt. To visualize the nucleus, a 1:1000 dilution of 10 mg/ml Hoechst 33258 in PBS was applied for 15 min at rt. Cells were then washed with PBS 5 times and imaged with a SP2 confocal microscope.

Migration assays. B16F10 cells (~75'000) were seeded in 24 well plates for 4 h. The media was replaced with starvation medium (0% FCS) in the presence or absence of 5μM Zn-DIGP and incubated overnight. Used media was then replaced by PBS and a scratch was made with sterile pipette tip and the detached cells were removed. Starvation media containing variable concentrations of CXCL10 or CXCL10 + 5 μM of Zn-DIGP was added to the cells. Bright field images with 4x objective were taken immediately after the scratch and after 24 h of incubation. The area of scratch was calculated using Image J software. The migration index is defined as the ratio of the area of scratch made at time 0 h to the area of scratch at 24 h.

Associated Content

Supporting Information Available: Synthesis and characterization of compounds **3** – **5**, as well as detailed protocols for microarray analyses, qRT-PCR and ELISA are included in supporting information. This material is available free of charge via the Internet at http://pubs.acs.org.

Acknowledgements

This work was made possible by generous support from the Swiss National Science Foundation (grant #130074) The authors thank the University of Zürich Center for Microscopy, Functional Genomics Center Zürich, and the Institute of Molecular Cancer Research for technical assistance. Animal care by S. Ressegatti is gratefully acknowledged. We also thank K. Italiano (EMD Millipore Corporation) for technical assistance with the CXCL10 radioligand displacement and Ca^{+2} flux assays.

References

1. Linos, E., Swetter, S. M., Cockburn, M. G., Colditz, G. A., and Clarke, C. A. (2009) Increasing burden of melanoma in the United States, *J Invest Dermatol 129*, 1666-1674.
2. Greenlee, R. T., Hill-Harmon, M. B., Murray, T., and Thun, M. (2001) Cancer statistics, 2001, *CA Cancer J Clin 51*, 15-36.

3. Wargo, J. A., and Tanabe, K. (2009) Surgical management of melanoma, *Hematol Oncol Clin North Am 23*, 565-581,
4. Brown, S. B., Brown, E. A., and Walker, I. (2004) The present and future role of photodynamic therapy in cancer treatment, *Lancet Oncol 5*, 497-508.
5. Sheleg, S. V., Zhavrid, E. A., Khodina, T. V., Kochubeev, G. A., Istomin, Y. P., Chalov, V. N., and Zhuravkin, I. N. (2004) Photodynamic therapy with chlorin e(6) for skin metastases of melanoma, *Photodermatol Photoimmunol Photomed 20*, 21-26.
6. Fasanella, K. E., and McGrath, K. (2009) Successful palliative treatment of duodenal metastatic melanoma with photodynamic therapy, *Gastrointestinal Endoscopy 69*, 182-184.
7. Robertson, C. A., Evans, D. H., and Abrahamse, H. (2009) Photodynamic therapy (PDT): a short review on cellular mechanisms and cancer research applications for PDT, *J Photochem Photobiol B 96*, 1-8.
8. De Rosa, F. S., and Bentley, M. V. (2000) Photodynamic therapy of skin cancers: sensitizers, clinical studies and future directives, *Pharm Res 17*, 1447-1455.
9. Allison, R. R., Downie, G. H., Cuenca, R., Hu, X.-H., Childs, C. J. H., and Sibata, C. H. (2004) Photosensitizers in clinical PDT, *Photodiagnosis and Photodynamic Therapy 1*, 27 - 42.
10. Cordoba, F., Braathen, L. R., Weissenberger, J., Vallan, C., Kato, M., Nakashima, I., Weis, J., and von Felbert, V. (2005) 5-aminolaevulinic acid photodynamic therapy in a transgenic mouse model of skin melanoma, *Experimental Dermatology 14*, 429-437.
11. Karunakaran, S. C., Babu, P. S., Madhuri, B., Marydasan, B., Paul, A. K., Nair, A. S., Rao, K. S., Srinivasan, A., Chandrashekar, T. K., Rao, C. M., Pillai, R., and Ramaiah, D. (2012) In vitro demonstration of apoptosis-mediated photodynamic activity and NIR nucleus imaging through a novel porphyrin, *ACS Chem Biol*. *8*, 127-132.
12. Kato, H., Furukawa, K., Sato, M., Okunaka, T., Kusunoki, Y., Kawahara, M., Fukuoka, M., Miyazawa, T., Yana, T., Matsui, K., Shiraishi, T., and Horinouchi, H. (2003) Phase II clinical study of photodynamic therapy using mono-L-aspartyl chlorin e6 and diode laser for early superficial squamous cell carcinoma of the lung, *Lung Cancer 42*, 103-111.
13. Tekdas, D. A., Kumru, U., Gurek, A. G., Durmus, M., Ahsen, V., and Dumoulin, F. (2012) Towards near-infrared photosensitisation: a photosensitising hydrophilic non-peripherally octasulfanyl-substituted Zn phthalocyanine, *Tetrahedron Letters 53*, 5227-5230.
14. Leznoff, C.C., Lever, A. B. P. (1989–1996) *Phthalocyanines-properties and applications*, VCH, New York, vol. I–IV.
15. Huang, Y., Xu, G., Peng, Y., Lin, H., Zheng, X., and Xie, M. (2007) Zinc phthalocyanine tetrasulfonate (ZnPcS4): a new photosensitizer for photodynamic therapy in choroidal neovascularization, *J Ocul Pharmacol Ther 23*, 377-386.
16. Baron, E. D., Malbasa, C. L., Santo-Domingo, D., Fu, P., Miller, J. D., Hanneman, K. K., Hsia, A. H., Oleinick, N. L., Colussi, V. C., and Cooper, K. D. Silicon phthalocyanine (Pc 4) photodynamic therapy is a safe modality for cutaneous neoplasms: results of a phase 1 clinical trial, *Lasers Surg Med 42*, 728-735.
17. Kimani, S.G., Shmigol, T.A., Hammond, S., Phillips, J.B., Bruce, J.I., Macrobert, A.J., Malakhov, M.V., Golding, J.P. (2013) Fully protected glycosylated zinc (II) phthalocyanine shows high uptake and photodynamic cytotoxicity in MCF-7 cancer cells, *Photochem Photobiol 89*, 139-149.

18. Dumoulin, F., Durmus, M., Ahsen, V., and Nyokong, T. (2010) Synthetic pathways to water-soluble phthalocyanines and close analogs, *Coordinaion Chemistry Reviews 254*, 2792-2847.
19. Alzeer, J., Roth, P. J., and Luedtke, N. W. (2009) An efficient two-step synthesis of metal-free phthalocyanines using a Zn(II) template, *Chem Commun (Camb)*, 1970-1971.
20. Alzeer, J., Vummidi, B. R., Roth, P. J., and Luedtke, N. W. (2009) Guanidinium-modified phthalocyanines as high-affinity G-quadruplex fluorescent probes and transcriptional regulators, *Angew Chem Int Ed Engl 48*, 9362-9365.
21. Membrino, A., Paramasivam, M., Cogoi, S., Alzeer, J., Luedtke, N. W., and Xodo, L. E. (2010) Cellular uptake and binding of guanidine-modified phthalocyanines to KRAS/HRAS G-quadruplexes, *Chem Commun (Camb) 46*, 625-627.
22. Papassava, P., Gorgoulis, V. G., Papaevangeliou, D., Vlahopoulos, S., van Dam, H., and Zoumpourlis, V. (2004) Overexpression of activating transcription factor-2 is required for tumor growth and progression in mouse skin tumors, *Cancer Res 64*, 8573-8584.
23. Miethe J, S. C., Wottrich K, Wenning D, Klempnauer KH. (2001) Crosstalk between Myc and activating transcription factor 2 (ATF2): Myc prolongs the half-life and induces phosphorylation of ATF2., *Oncogene 20*, 8116-8124.
24. Zhuang D, M. S., Grachtchouk V, Tang WH, Patil S, Wawrzyniak JA, Berman AE, Giordano TJ, Prochownik EV, Soengas MS, Nikiforov MA. (2008) C-MYC overexpression is required for continuous suppression of oncogene-induced senescence in melanoma cells., *Oncogene 27*, 6623-6634.
25. Walser, T. C., Rifat, S., Ma, X., Kundu, N., Ward, C., Goloubeva, O., Johnson, M. G., Medina, J. C., Collins, T. L., and Fulton, A. M. (2006) Antagonism of CXCR3 inhibits lung metastasis in a murine model of metastatic breast cancer, *Cancer Res 66*, 7701-7707.
26. Wijtmans, M., Verzijl, D., Leurs, R., de Esch, I. J., and Smit, M. J. (2008) Towards small-molecule CXCR3 ligands with clinical potential, *ChemMedChem 3*, 861-872.
27. Cambien, B., Karimdjee, B. F., Richard-Fiardo, P., Bziouech, H., Barthel, R., Millet, M. A., Martini, V., Birnbaum, D., Scoazec, J. Y., Abello, J., Al Saati, T., Johnson, M. G., Sullivan, T. J., Medina, J. C., Collins, T. L., Schmid-Alliana, A., and Schmid-Antomarchi, H. (2009) Organ-specific inhibition of metastatic colon carcinoma by CXCR3 antagonism, *Br J Cancer 100*, 1755-1764.
28. Wender, P. A., Galliher, W. C., Goun, E. A., Jones, L. R., and Pillow, T. H. (2008) The design of guanidinium-rich transporters and their internalization mechanisms, *Advanced Drug Delivery Reviews 60*, 452-472.
29. Griffiths, J., Cruse-Sawyer, J., Wood, S. R., Schofield, J., Brown, S. B., and Dixon, B. (1994) On the photodynamic therapy action spectrum of zinc phthalocyanine tetrasulphonic acid in vivo, *J Photochem Photobiol B 24*, 195-199.
30. Spikes, J. D., and Bommer, J. C. (1986) Zinc tetrasulphophthalocyanine as a photodynamic sensitizer for biomolecules, *Int J Radiat Biol Relat Stud Phys Chem Med 50*, 41-45.
31. Hirohara, S., Obata, M., Ogata, S., Kajiwara, K., Ohtsuki, C., Tanihara, M., and Yano, S. (2006) Sugar-dependent aggregation of glycoconjugated chlorins and its effect on photocytotoxicity in HeLa cells, *J Photochem Photobiol B 84*, 56-63.
32. Musil, Z., Zimcik, P., Miletin, M., Kopecky, K., Link, M., Petrik, P., and Schwarz, J. (2006) Synthesis and singlet oxygen production of azaphthalo-cyanines bearing

functional derivatives of carboxylic acid, *Journal of Porphyrins and Phthalocyanines 10*, 122-131.
33. Kuznetsova, N. A., Gretsova, N. S., Derkacheva, V. M., Kaliya, O. L., and Lukyanets, E. A. (2003) Sulfonated phthalocyanines: aggregation and singlet oxygen quantum yield in aqueous solutions, *Journal of Porphyrins and Phthalocyanines 7*, 147-154.
34. De Rosa, M. C., and Cruthcley, R. J. (2002) Photosensitized singlet oxygen and its applications, *Coordination Chemistry Reviews 233*, 354-371.
35. Jensen, N. A., Pedersen, K. M., Lihme, F., Rask, L., Nielsen, J. V., Rasmussen, T. E., and Mitchelmore, C. (2003) Astroglial c-Myc overexpression predisposes mice to primary malignant gliomas, *J Biol Chem 278*, 8300-8308.
36. Zhang, X., Lee, C., Ng, P. Y., Rubin, M., Shabsigh, A., and Buttyan, R. (2000) Prostatic neoplasia in transgenic mice with prostate-directed overexpression of the c-myc oncoprotein, *Prostate 43*, 278-285.
37. Schultz, J., Pavlovic, J., Strack, B., Nawrath, M., and Moelling, K. (1999) Long-lasting anti-metastatic efficiency of interleukin 12-encoding plasmid DNA, *Hum Gene Ther 10*, 407-417.
38. Noreen, F., Heinrich, J., and Moelling, K. (2009) Antitumor activity of small double-stranded oligodeoxynucleotides targeting telomerase RNA in malignant melanoma cells, *Oligonucleotides 19*, 169-178.
39. Pandha, H. S., Heinemann, L., Simpson, G. R., Melcher, A., Prestwich, R., Errington, F., Coffey, M., Harrington, K. J., and Morgan, R. (2009) Synergistic effects of oncolytic reovirus and cisplatin chemotherapy in murine malignant melanoma, *Clin Cancer Res 15*, 6158-6166.
40. Sun, D., Guo, K., and Shin, Y. J. (2011) Evidence of the formation of G-quadruplex structures in the promoter region of the human vascular endothelial growth factor gene, *Nucleic Acids Research 39*, 1256-1265.
41. Xu, Y., and Sugiyama, H. (2006) Formation of the G-quadruplex and i-motif structures in retinoblastoma susceptibility genes (Rb), *Nucleic Acids Research 34*, 949-954.
42. Lee, J. H., Kim, H. N., Kim, K. O., Jin, W. J., Lee, S., Kim, H. H., Ha, H., and Lee, Z. H. (2012) CXCL10 promotes osteolytic bone metastasis by enhancing cancer outgrowth and osteoclastogenesis, *Cancer Res 72*, 3175-3186.
43. Booth, V., Keizer, D. W., Kamphuis, M. B., Clark-Lewis, I., and Sykes, B. D. (2002) The CXCR3 binding chemokine IP-10/CXCL10: structure and receptor interactions, *Biochemistry 41*, 10418-10425.
44. Jabeen, T., Leonard, P., Jamaluddin, H., and Acharya, K. R. (2008) Structure of mouse IP-10, a chemokine, *Acta Crystallogr D Biol Crystallogr 64*, 611-619.
45. Heise, C. E., Pahuja, A., Hudson, S. C., Mistry, M. S., Putnam, A. L., Gross, M. M., Gottlieb, P. A., Wade, W. S., Kiankarimi, M., Schwarz, D., Crowe, P., Zlotnik, A., and Alleva, D. G. (2005) Pharmacological characterization of CXC chemokine receptor 3 ligands and a small molecule antagonist, *J Pharmacol Exp Ther 313*, 1263-1271.
46. Sauty, A., Colvin, R. A., Wagner, L., Rochat, S., Spertini, F., and Luster, A. D. (2001) CXCR3 internalization following T cell-endothelial cell contact: preferential role of IFN-inducible T cell alpha chemoattractant (CXCL11), *J Immunol 167*, 7084-7093.
47. Meiser, A., Mueller, A., Wise, E. L., McDonagh, E. M., Petit, S. J., Saran, N., Clark, P. C., Williams, T. J., and Pease, J. E. (2008) The chemokine receptor CXCR3 is degraded

following internalization and is replenished at the cell surface by de novo synthesis of receptor, *J Immunol 180*, 6713-6724.
48. Kawada, K., Sonoshita, M., Sakashita, H., Takabayashi, A., Yamaoka, Y., Manabe, T., Inaba, K., Minato, N., Oshima, M., and Taketo, M. M. (2004) Pivotal role of CXCR3 in melanoma cell metastasis to lymph nodes, *Cancer Res 64*, 4010-4017.
49. Martins, V. L., Vyas, J. J., Chen, M., Purdie, K., Mein, C. A., South, A. P., Storey, A., McGrath, J. A., and O'Toole, E. A. (2009) Increased invasive behaviour in cutaneous squamous cell carcinoma with loss of basement-membrane type VII collagen, *J Cell Sci 122*, 1788-1799.
50. Yoshida, R., Nagira, M., Kitaura, M., Imagawa, N., Imai, T., and Yoshie, O. (1998) Secondary lymphoid-tissue chemokine is a functional ligand for the CC chemokine receptor CCR7, *J Biol Chem 273*, 7118-7122.
51. Bhatia, S., Tykodi, S. S., and Thompson, J. A. (2009) Treatment of metastatic melanoma: an overview, *Oncology (Williston Park) 23*, 488-496.
52. Cubeddu, R., Canti, G., Musolino, M., Pifferi, A., Taroni, P., and Valentini, G. (1996) In vivo absorption spectrum of disulphonated aluminium phthalocyanine in a murine tumour model, *J Photochem Photobiol B 34*, 229-235.
53. Wendel, M., Galani, I. E., Suri-Payer, E., and Cerwenka, A. (2008) Natural killer cell accumulation in tumors is dependent on IFN-gamma and CXCR3 ligands, *Cancer Res 68*, 8437-8445.
54. Saudemont, A., Jouy, N., Hetuin, D., and Quesnel, B. (2005) NK cells that are activated by CXCL10 can kill dormant tumor cells that resist CTL-mediated lysis and can express B7-H1 that stimulates T cells, *Blood 105*, 2428-2435.
55. Antonicelli, F., Lorin, J., Kurdykowski, S., Gangloff, S. C., Le Naour, R., Sallenave, J. M., Hornebeck, W., Grange, F., and Bernard, P. (2011) CXCL10 reduces melanoma proliferation and invasiveness in vitro and in vivo, *Br J Dermatol 164*, 720-728.
56. Pfeiffer, R., Kirsch, J., and Fahrenholz, F. (1998) Agonist and antagonist-dependent internalization of the human vasopressin V2 receptor, *Exp Cell Res 244*, 327-339.
57. Pheng, L. H., Dumont, Y., Fournier, A., Chabot, J. G., Beaudet, A., and Quirion, R. (2003) Agonist- and antagonist-induced sequestration/internalization of neuropeptide Y Y1 receptors in HEK293 cells, *Br J Pharmacol 139*, 695-704.

Table 1

No	Compound	Φ for emission	Φ for $^1O_2$	EC_{50} for toxicity (μM)	
				(-) laser	(+) laser
1	DIGP	0.26	0.06 ± .008	25 ± 5	32 ± 6
2	Zn-DIGP	0.28	0.51 ± .05	>80	0.16 ± .08
3	Cu-DIGP	< 0.001	0.03 ± 0.006	>80	> 80
4	Co-DIGP	< 0.001	< 0.01	>80	>80
5	Pd-DIGP	0.002	0.41 ± .02	>80	2.1 ± .14
6	Zn-Pc	0.34	0.61	ND	ND
7	Zn-PcS4	0.29	0.50 ± .04	>80	2.7 ± 0.5

Table legend

Table 1 Quantum yields (Φ) for singlet oxygen and luminescence of phthalocyanines **1** – **7**. EC_{50} values for B16F10 cells were determined in the absence of light (**-***hv*) or following a 90 second exposure to red laser light (+*hv*) at 660 nm. EC_{50} values for compound **6** were not determined "ND" due to its poor solubility properties in aqueous media.

Figure legends

Figure 1 Structures of tetrakis-diisopropyl-guanidine-phthalocyanine (DIGP) derivatives containing various metal ions "M", and the reference compounds zinc phthalocyanine (ZnPc) and zinc phthalocyanine tetrasulfonate (Zn-PcS4).

Figure 2 Cellular uptake of Zn-DIGP into living B16F10 cells before (**A** – **C**) and after (**D** – **F**) a 90 second exposure to red laser light at 660 nm. (**A**, **D**) Brightfield images. (**B**, **E**) Fluorescence

emission from Zn-DIGP (Ex = 620 nm, Em = 700 nm). (**C**) Composite image of (**A** – **B**). (**F**) Composite image of (**D – E**). Scale bars represent 30 μm.

Figure 3 (**A**) Cellular respiration of B16F10 cells treated with Zn-DIGP and kept in the dark (**-** laser) as compared to Zn-DIGP-treated cells irradiated with 20 joules of 660 nm laser light (+ laser) (**B**) Photobleaching of DPBF absorbance in the presence of **1** – **7** upon irradiation at 660 nm.

Figure 4 *In vivo* effects of Zn-DIGP on melanoma colony formation in lung tissues of C57BL/6 mice. "Type A" experiments indicate intravenous injection of B16F10 cells pre-treated with Zn-DIGP. "Type B" experiments indicate direct intravenous injection of Zn-DIGP 24 hours after injection of B16F10 cells. Vertical bars represent the mean number and standard error of tumor colonies present in lungs on day 20. *** and ** represent $p < 0.001$ and $p < 0.01$, respectively.

Figure 5 Relative CXCL10 mRNA abundance in B16F10 cells with respect to untreated cells according to qRT-PCR. (**A**) CXCL10 mRNA versus Zn-DIGP concentrations after 24 hours. (**B**) Time-dependent changes in the presence of 5 μM of Zn-DIGP. All qRT-PCR values were normalized to two different housekeeping genes (β-actin and SDHA). Error bars indicate standard errors.

Figure 6 Changes in extracellular CXCL10 protein concentrations according to ELISA. (**A**) CXCL10 versus Zn-DIGP concentrations after 24 hours. (**B**) Time-dependent changes in the presence of 5 μM of Zn-DIGP. Error bars indicate standard errors.

Figure 7 (**A**) ^{125}I-CXCL10 displacement following a 2 hour incubation with unlabeled CXCL10 or Zn-DIGP. (**B**) CXCR3 receptor activation by CXCL10 and Zn-DIGP in Chem 1 cells according to intra-cellular calcium levels. (**C**) Inhibition of CXCL10-mediated CXCR3 receptor activation by Zn-DIGP in Chem1 cells according to intra-cellular calcium levels.

Figure 8 Confocal microscopy images of B16F10 cells stained for CXCR3 after addition of Zn-DIGP (5 μM) or CXCL10 (20 nM). Green staining represents the CXCR3 specific antibody and blue staining represent nucleus specific Hoechst 33258. (**A**) – (**C**) are images taken at t = 0 of incubation, (**D**) – (**F**) are images taken after 1 hour following the addition of CXCL10 and Zn-DIGP. (**G**) – (**I**) are images taken after 2 hours. In all cases, cells were fixed prior to imaging, and the same detector gain and laser intensities were used on the microscope. Scale bars represent 30 μM.

Figure 9 (**A**) Bright field images of scratches made in monolayers of B16F10 cells. A) & B) are images taken immediately after addition of Zn-DIGP and/or CXCL10. C) & D) are images taken after 24h. Scale bars represent 50 mm. (**B**) Summary of scratch assay results where migration index is defined as the ratio of the area of scratch at 0 h versus 24 h. "Untreated" indicates addition of CXCL10 or CCL21 only. A migration index of 1.0 corresponds to the cellular migration in the absence of added chemokine.

Figure 1

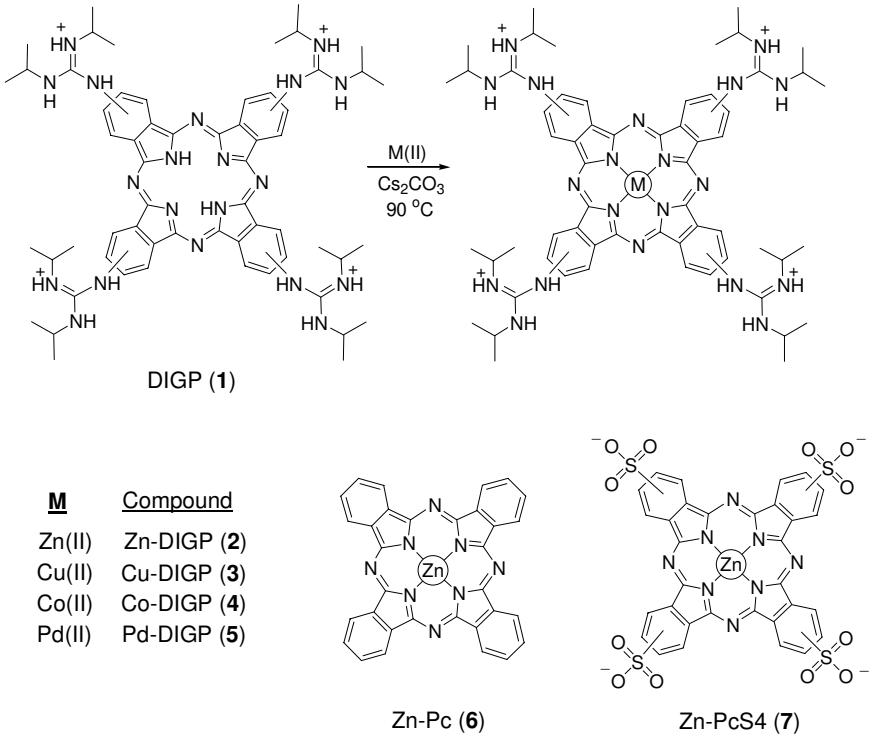

Figure 2

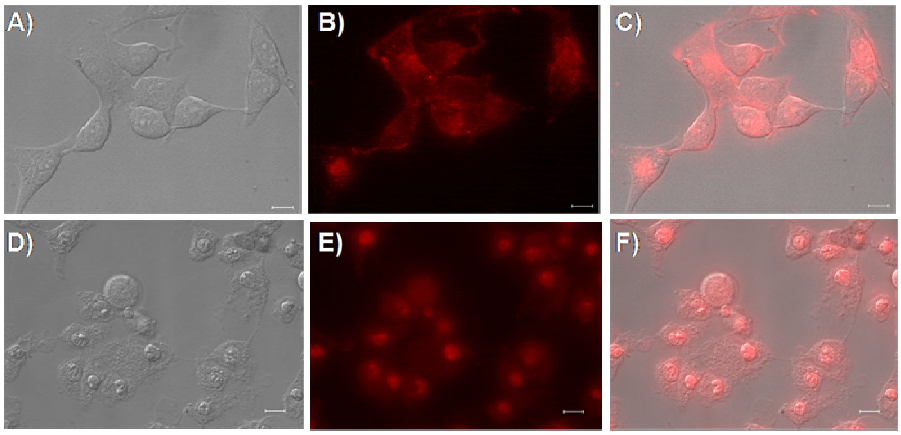

Figure 3

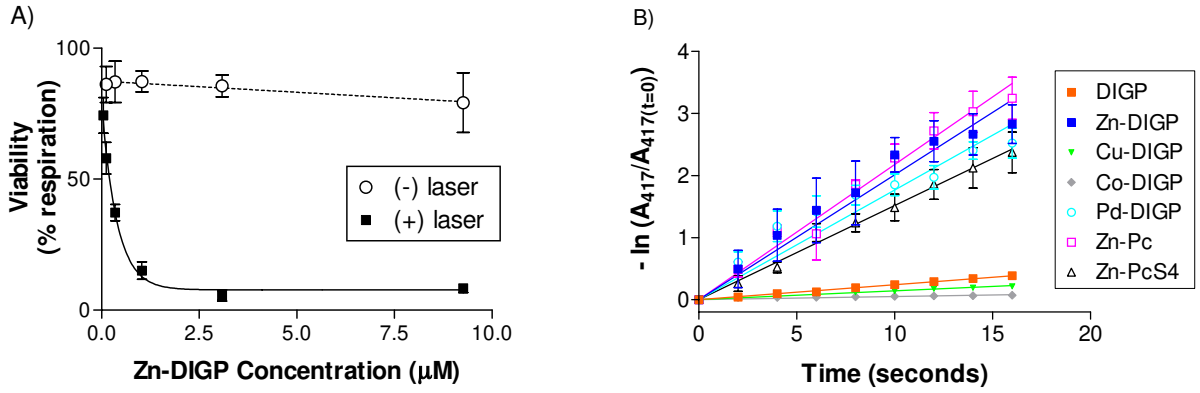

Figure 4

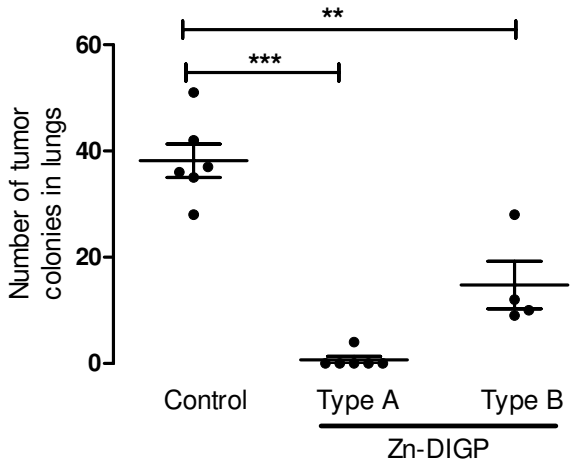

Figure 5

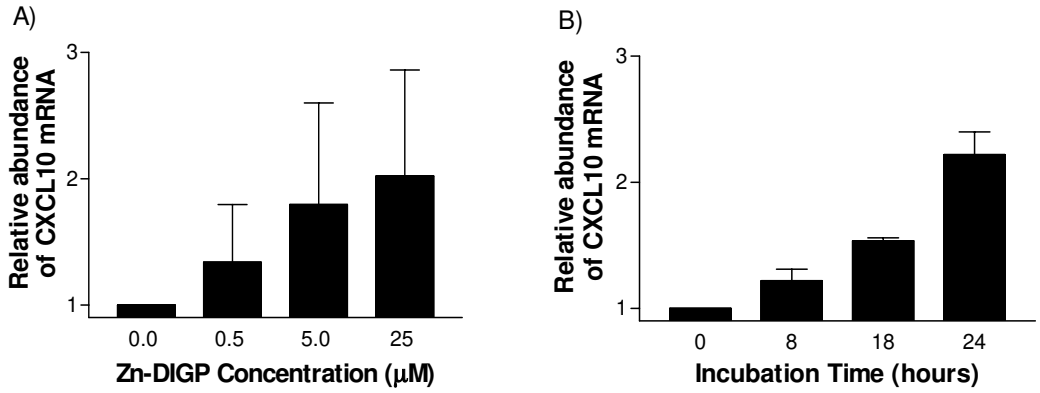

Figure 6

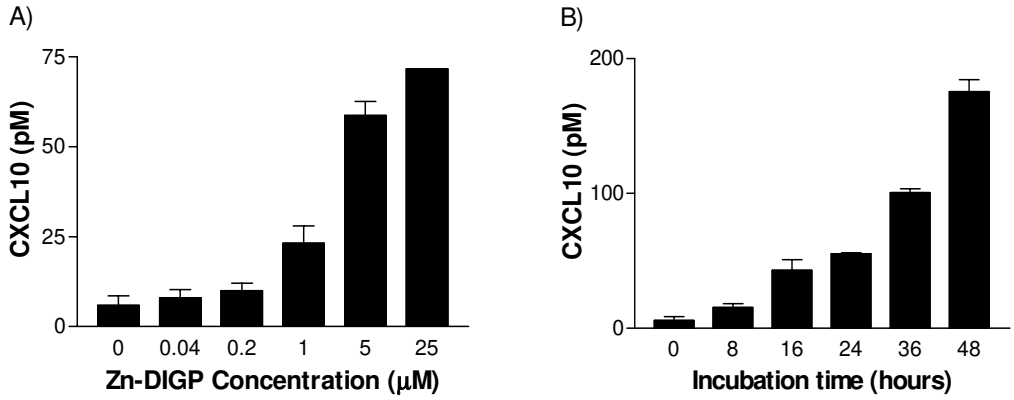

Figure 7

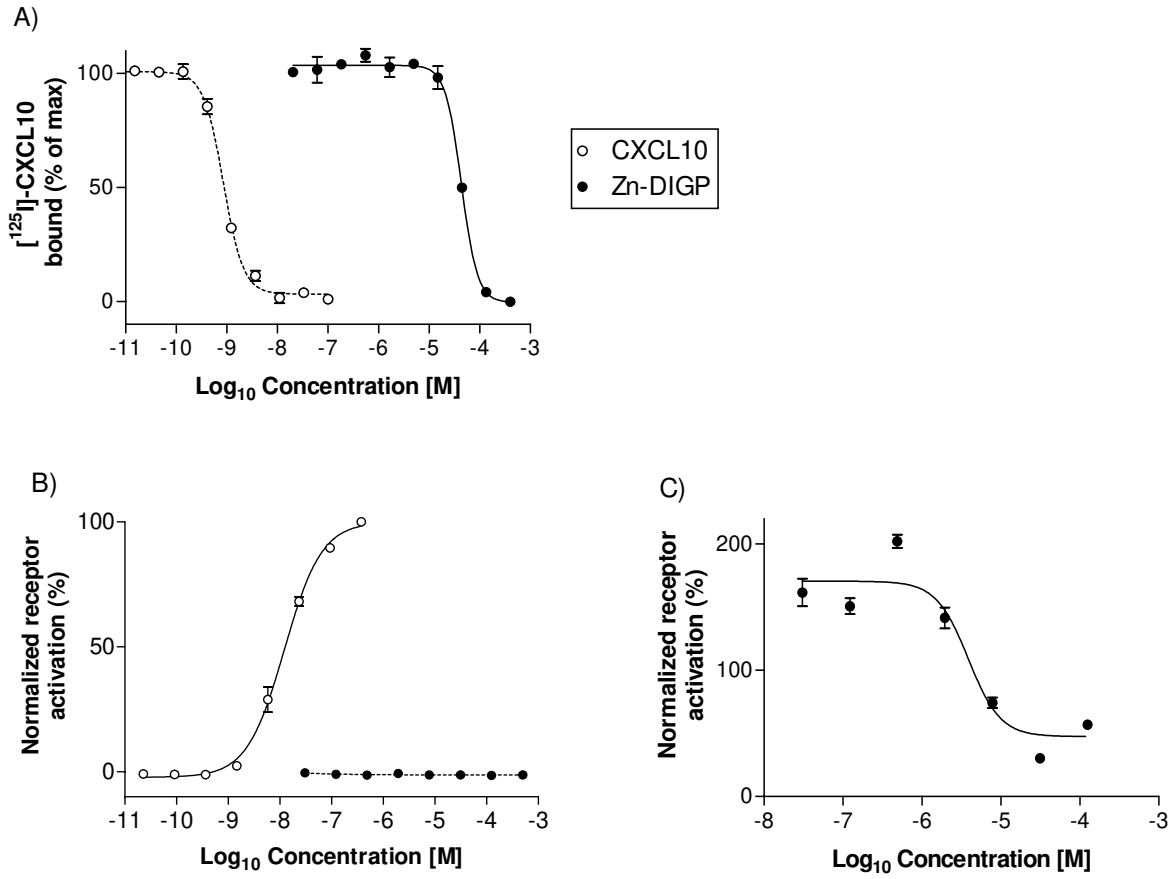
A)
100
50
0
-11 -10 -9 -8 -7 -6 -5 -4 -3
[125I]-CXCL10 bound (% of max)
Log10 Concentration [M]
CXCL10
Zn-DIGP
B)
100
50
0
-11 -10 -9 -8 -7 -6 -5 -4 -3
Normalized receptor activation (%)
Log10 Concentration [M]
C)
200
100
0
-8 -7 -6 -5 -4 -3
Normalized receptor activation (%)
Log10 Concentration [M]

Figure 8

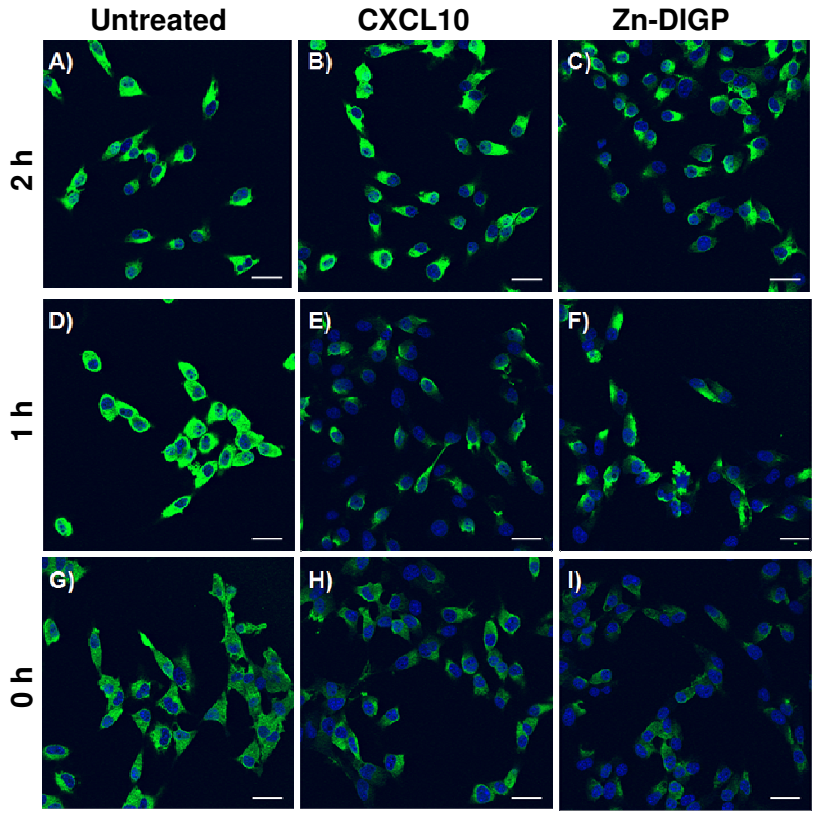

Figure 9

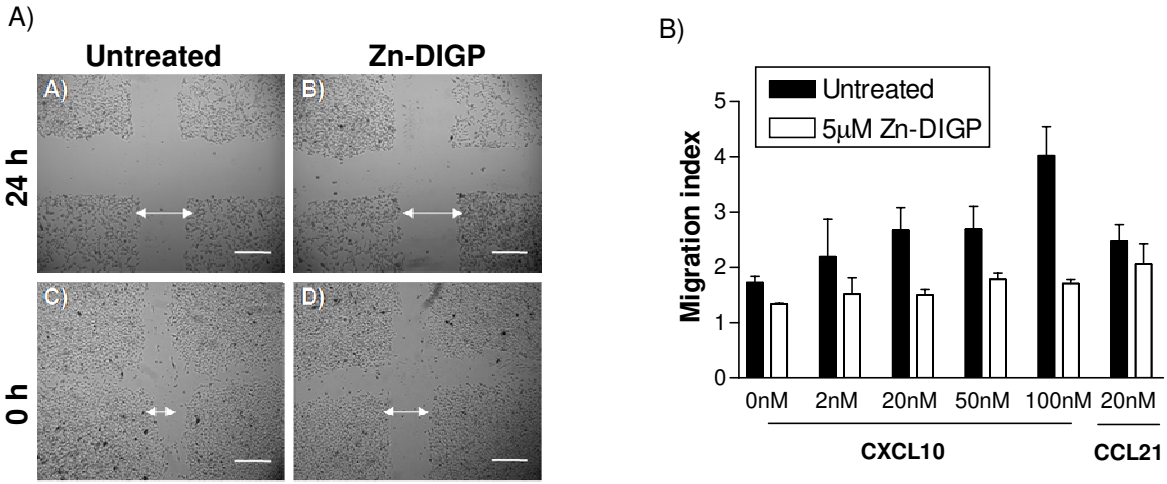

Graphical abstract